January 2008

Visualization of Groundwater Flow within Touching-Vu and Matrix Porosity in an Eogenetic Karst Aquifer

Lee J. Florea
Western Kentucky University, lflorea@bsu.edu

Kevin J. Cunningham
US Geological Survey

Stephen Altobelli
New Mexico Resonance

Visualization of Groundwater Flow Within Touching-Vug and Matrix Porosity in an Eogenetic Karst Aquifer

Lee J. Florea
Kevin J. Cunningham
U.S. Geological Survey, FISC-Fort Lauderdale
3110 SW 9th Ave.,
Ft. Lauderdale, FL 33315
lflorea@usgs.gov
kcunning@usgs.gov

Stephen Altobelli
New Mexico Resonance
2301 Yale Blvd. SE, Suite C-1,
Albuquerque, NM 87106
salto@nmr.org

INTRODUCTION

In this study, we use an innovative, non-invasive technology, nuclear magnetic resonance imaging (NMRI), to visualize the direction and magnitude of groundwater flow in field samples of late Pleistocene limestone of the Biscayne aquifer. Specific goals of the first set of NMRI experiments are to map the advective velocity of water flowing at two rates of specific discharge (0.00025 and 0.00013 m/s) through a 10-cm-diameter cylindrical, epoxy-resin model. The model interior accurately reproduces a well-connected maze of ichnologically influenced, centimeter-scale, touching-vug macroporosity common within preferred flow zones in parts of the Biscayne aquifer. A second set of NMRI experiments investigates the migration of freshwater into the matrix of permeable and porous peloid-ooid grainstone initially saturated with heavy water (D_2O). In the experiments on the physical model, we generate the velocity maps using phase-encoded, stimulated-echo imaging. In the experiments on the rock matrix, we visualize the progressive displacement of D_2O in the rock matrix using sequential time-step images of NMRI signal strength.

Results for the freshwater-D_2O experiments reveal a substantial flux of freshwater into the matrix porosity with a simultaneous loss of D_2O. Specifically, we measured rates upward of 0.001 milliliters per hour per gram of sample (mL/hr-g) in static or non-flowing conditions. We also measured rates as great as 0.07 mL/hr-g when freshwater continuously flows past a sample at velocities less than those found within stressed areas of the Biscayne aquifer. These experiments illustrate how freshwater and D_2O, with different chemical properties, migrate within one type of matrix porosity found in the Biscayne aquifer. Furthermore, these experiments are a comparative exercise in the displacement of seawater by freshwater in the matrix of a coastal, karst aquifer, since D_2O has a greater density than freshwater.

HYDROGEOLOGY OF THE BISCAYNE AQUIFER

The unconfined Biscayne aquifer of southeast Florida (Fish and Stewart, 1991) is among the most permeable aquifers in the world (Parker et al., 1955) with a range in hydraulic conductivities between 0.00000035 and >0.0035 m/s (Fish and Stewart, 1991, Plates 1-11) and an ambient hydraulic gradient of 0.0001-0.000001 (approximated from Figure 18 of Fish and Stewart, 1991). Pleistocene limestone of the Fort Thompson Formation, including the Miami Limestone deposited during the last Pleistocene interglacial period (Marine Isotope Stage 5e), is the dominant rock that composes the Biscayne aquifer (Fish and Stewart, 1991). Our samples of the Miami Limestone (ML-1, ML-2, and ML-3) are peloid-ooid grainstones that come from an outcrop near Biscayne Bay. The limestones of the Biscayne aquifer are overprinted with eogenetic, meteoric diagenesis and karstification (Vacher and Mylroie, 2002; Cunningham, 2004; Cunningham et al., 2006a,b).

Recently, Cunningham et al. (2004a,b; 2006a,b) used geologic and geophysical data from about 71 coreholes within a roughly 230-km^2 study area in Miami-Dade County to develop a three-dimensional conceptual hydrostratigraphic model of the Biscayne aquifer. Those data, including surface geophysics (Cunningham et al., 2004a,b), stratigraphic profiles, borehole flowmeter measurements, and results of tracer experiments (Renken et al., 2005a), demonstrate that macroporosity and groundwater flow are commonly concentrated within stratigraphic cycles and are closely linked to vertical lithofacies

successions composing the cycles within the Fort Thompson Formation and Miami Limestone. The macroporosity is commonly stratiform, with tabular-shaped mazes of centimeter-scale touching vugs (Renken et al., 2005a; Cunningham et al., 2004a,b; 2006a,b). Macropores are either separate or linked as touching vugs (terminology of Lucia, 1995).

Digital optical borehole images of borehole walls, combined with recovered core and field specimens from outcrop, indicate that the preponderance of the touching vugs is biogenic macroporosity. Biogenic macroporosity largely manifests as: (1) ichnogenic macroporosity primarily related to post-depositional burrowing activity by callianassid shrimp; and (2) biomoldic macroporosity originating by dissolution of fossil hard parts, principally mollusk shells (Cunningham and Curran, 2007). Most of the ichnologically related macroporosity in the limestone of the Biscayne aquifer is associated with an *Ophiomorpha* ichnofabric. *Ophiomorpha* are common in Pleistocene limestone of the Caribbean and south Florida (Curran, 2007). At outcrop, locals refer to maximum-intensity Ophiomorpha ichnofabric as "lace rock." Cavers, referring to their physical distress while crawling through local caves, call this ichnofabric "razor rock" (Cressler, 1993, Figure 1). Perhaps the most fitting visual analogy for dense occurrences of *Ophiomorpha* comes from the realm of fiction, when, in The Golden Compass, Philip Pullman uses the phrase "froth of stone" (Pullman, 2007, p. 36).

The Biscayne aquifer is not a karst aquifer sensu classico. Although cavernous voids common to the Upper Floridan aquifer (Florea et al., 2007) are indeed present in the Biscayne aquifer (Cressler 1993, Figure 1), large-scale regional cavernous porosity and associated conduit flow, such as in the Yucatan

Figure 1. A thick zone of the ***Ophiomorpha*** ichnofabric or "razor rock" in Fat Sleeper Cave, located near Biscayne Bay south of downtown Miami (photo by Alan Cressler).

(Smart et al., 2006), have not been documented beyond their suggested presence by Parker et al. (1955). This particular difference strikes a strong contrast to the pipe-like conceptual models of the kind that rule the present view of karst aquifers and is hydrologically similar to other forms of karst aquifers in which caves have formed in a non-conduit flow field – namely banana holes and flank margin caves within carbonate island aquifers (Mylroie et al., 1995).

However, the hydrology of the Biscayne aquifer behaves in most every way as a dual-porosity karst aquifer. For example, Renken et al. (2005a), within the study area of Cunningham et al. (2004a,b; 2006a,b), performed a forced-gradient tracer test in a large municipal well field using the conservative tracers, rhodamine WT and deuterium. Low relative dispersivity and a rapid flow rate with an approximate mean velocity of 386 m/day (0.0045 m/s) (Renken et al., 2005a) characterized the trace with the fastest flow path probably dominated by an Ophiomorpha ichnofabric.

Moreover, the limestone composing the Biscayne aquifer commonly has substantial primary interparticle and secondary moldic porosity. One effect is that groundwater storage is considerable within the matrix porosity (e.g., Worthington et al., 2000). Markedly different from telogenetic karst is the relative contribution that the matrix porosity can contribute to groundwater flow in eogenetic karst (Budd and Vacher, 2004). Furthermore, the accessibility of matrix storage to fluids within the macroporous part of eogenetic karst aquifers has been exemplified for the unconfined Floridan aquifer (Martin and Dean, 2001; Florea and Vacher, 2006). Finally, the spatial variation of the permeability of matrix porosity in an eogenetic karst aquifer can markedly influence the pathways of preferential groundwater flow (Vacher et al., 2006; Budd and Vacher, 2004). In the Upper Floridan aquifer, these heterogeneities in matrix permeability are abundant (Budd and Vacher, 2004) and may span more than an order of magnitude on the scale of a hand specimen (Chapter 4 of Florea, 2006).

In summary, we conceptualize the Biscayne aquifer in the study area of Cunningham et al. (2004a,b; 2006a, b) as a dual-porosity system consisting of (1) a matrix porosity of interparticle and separate vugs and (2) touching-vug porosity that is commonly ichnologically influenced or composed of fossil molds. The touching-vug porosity commonly manifests as stratiform, areally extensive horizons. Bedding-plane and cavernous vugs, and vertical solution pipes are less important in terms of groundwater flow.

At the scale of a field specimen, groundwater flow in the Biscayne aquifer through a maze of touching vugs related to the

trace fossil Ophiomorpha or other forms of ichnologically related porosity is a multifaceted hydrologic problem. For example, flow paths are tortuous and groundwater flow diverges and reassembles throughout the network of touching vugs. Additionally, the matrix porosity may act as a sponge, retaining and releasing solutes over time. In this paper, we present innovative methodologies of imaging, prototyping, and visualization to investigate the complex hydrology of the matrix and macropores associated with our samples of the Miami Limestone.

SAMPLES AND MODEL DEVELOPMENT

Our goal in this study is to investigate the character of two forms of groundwater flow in the Biscayne aquifer: 1) through the touching-vug porosity, and 2) the flux of freshwater between the matrix porosity and the surrounding touching vugs using samples initially saturated with deuterium oxide (D_2O). We use nuclear magnetic resonance imaging (NMRI) in all experiments to image groundwater flow in non-invasive manner.

Samples ML-1, ML-2, and ML-3 come from a stratiform zone of peloid-ooid grainstone that has an intense Ophiomorpha inchofabric and represent the end member of this ichnofabric with very high macroporosity. The samples are burrowed and free of interstitial sediment to the point that the limestone contains roughly equal proportions of macropores and limestone matrix as measured within ML-1 (Michael Sukop, per. comm.). The rock matrices of these samples are themselves porous and permeable. The mean matrix porosity on a sample from the same outcrop as both ML-2 and ML-3 measures 44% ($n = 4$, $\sigma = 5.4$) with a matrix permeability that ranges between $10^{-12.4}$ m^2, as measured using pressure decay on core plug, and $10^{-13.5}$ m^2 measured using a gas minipermeameter. Furthermore, that sample has a bulk density of 2.73 g/cm^3 (Table 1).

Groundwater flow in the touching vugs was realized by constructing a physical model using a rapid prototyping technology that reproduces the complex geometry of touching-vug porosity of sample ML-1. The movement of groundwater within the matrix porosity of samples ML-2 and ML-3 in our experiments occurred within the rocks themselves.

Imaging of sample ML-1 with X-ray computed tomography

The largest sample (ML-1; Figure 2A) was scanned at the High Resolution X-ray CT Facility at the Jackson School of Geosciences at the University of Texas at Austin. The X-ray source is a 200 kV FeinFocus model FXE200.20, with an image intensifier detector system from which data are captured and digitized by a CCD 1024X1024 camera (Ketcham and Iturrino, 2005). A facility, highly detailed, three-dimensional, non-destructiv age slices of the sample were obtained in the vertical p Each slice was 1.0 mm thick with a 0.2-mm overlap, to pro a 0.8 mm-interslice spacing. The CT images had a resoluti 0.271 mm in length and width per pixel.

The set of slices was reconstructed into a 3-dimensional file that measures 320 mm in the z-direction, 263 mm i x-direction, and 200 mm in the y-direction (Figure 2B). resulting digital file is viewable and editable with a varie visualization software packages. A cylinder with the long measuring 230 mm in the z-direction and 100 mm in bot x- and y-directions was cropped from the digital data (F 2C). Also within the software, a digital sheath of solid ma with a thickness of 1.8 mm was added to the exterior o cropped cylinder.

Prototype development from a digital ima of ML-1

We identified two particular types of rapid prototyping nologies with sufficient build envelopes that can accur reproduce the complexities of our dataset. The first techn produced by Z-Corp, Inc., fuses very thin layers of gyp with a glue sprayed, via inkjets, onto portions of the build that are part of the model. Compressed air removes gyp that is not fused to the final prototype. The second techn originally produced by Sanders Prototype, Inc., uses no to spray thin layers of epoxy where data exist in the mode wax where there are no data. A UV light cures the epoxy each layer is printed. After the printing is complete, a so removes the wax.

Other rapid prototyping technologies are unable to repro the complexities of the macroporous digital cylinder sh in Figure 2C. They cannot connect pendants or other han features to portions of the model already printed. These technologies include: stereolithography, in which ultrav laser radiation is directed onto a vat of polymer resin (li plastic); fused deposition modeling, which generates mo by extruding a controlled bead of molten polymer throu fine nozzle; and selective laser sintering, in which an obje created by sequentially fusing thin layers of a powder w scanning laser beam.

Of the two prototype methods appropriate for our needs selected the wax-epoxy method to produce our cylindrical model. The gypsum method, although accurate for our n and more representative of the porosity, texture, and ch

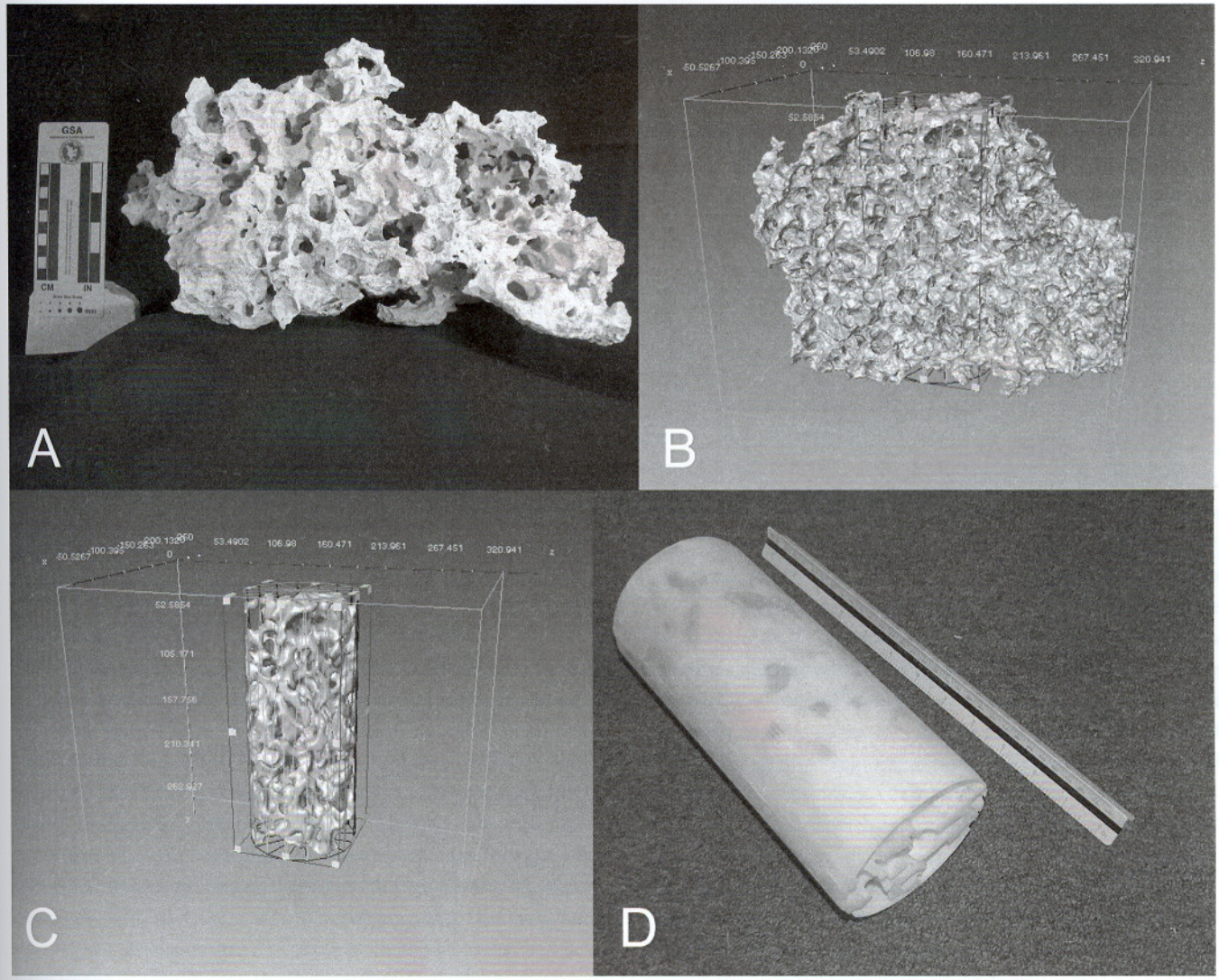

Figure 2. A) Sample ML-1, a peloid-ooid grainstone from the Miami Limestone with centimeter-scale, touching-vug porosity associated with *Ophiomorpha*. B) Digital reproduction of sample ML-1 using data from computed tomography (scale is in millimeters). C) Cylindrical crop of the digital data from ML-1 used for rapid prototyping (scale is in millimeters). D) Epoxy prototype produced using the cylinder of digital data presented in C (scale is in inches).

cal reactivity of the original rock, results in a physical model that is less durable. The epoxy-based system eliminates these concerns. The stated accuracy achievable with the wax-epoxy printer is +/- 0.01 mm/mm in the x-, y-, and z-directions, and features greater than 0.254 mm are resolvable. The resulting physical model accurately reproduces the detail of the Ophiomorpha ichnoporosity (Figure 2D).

FLOW VISUALIZATION USING NUCLEAR MAGNETIC RESONANCE IMAGING

We used NMRI to image water movement in all experiments. In the experiments on the physical model, we generated maps of velocity direction and magnitude. In the experiments on the rock matrix, we visualized the progressive displacement of D_2O in the rock matrix using sequential time-step images of NMRI signal strength.

NMRI measures the average precession of nuclear spins within a static magnetic field (Fukushima, 1999; Callaghan, 1991) and is increasingly a useful tool to study fluid flow within porous media (e.g., Chang and Watson, 1999; Seymour and Callaghan, 1997; Shattuck et al., 1997; Tessier et al., 1997). Freshwater is particularly suited for NMRI because it possesses protons in abundance. Trace amounts of gadopentetate dimeglumine (Gd-DTPA – $C_{28}H_{54}GdN_5O_{20}$), a medical contrast agent with a density of 1.195 g/mL, enhance the NMRI signal by shortening T1, the spin-lattice relaxation time, of freshwater while at the

same time not significantly increasing the density of the resulting mixture. In contrast, D_2O and carbonate rock produce little or no NMRI signal because they lack mobile protons.

In NMRI, the nuclear spins are not imaged in equilibrium alignment. Rather, a second magnetic field created by a radio-frequency, rf, pulse is tuned to the resonant, or Lamor, frequency,

$$\omega_0=\gamma B_0, \qquad (1)$$

where ω_0 is the Lamar frequency, B_0 is the field strength, and γ is a constant for the nuclear species (Callaghan, 1991) – 42.5 MHz/T for protons. A third set of magnetic fields, generated by gradient coils, causes the Lamor frequency to depend upon the location of the spin, or

$$\omega= \gamma(B_0 + \mathbf{r} \bullet \mathbf{G}), \qquad (2)$$

where **r** is the position vector and **G** is the vector of the gradient magnetic field. In this way, components of the position of an object may be determined. For several small objects (i.e., a group of water molecules), the signal of all objects as a function of time, S(t), is the volume integral of the product between the magnetization vector **M**(r) and the instantaneous phase of the magnetization φ(r,t),

$$S(t) = \int \mathbf{M}(r) e^{i\varphi(r,t)} dV, \qquad (3)$$

where φ(r,t) depends upon the history of all gradients and molecular motion following the resonance rf pulse that starts each NMR experiment (Fukushima, 1999; Callaghan, 1991). Taking the Fourier transform of S(t) reveals one component of the position for each small object in the experiment. In our case, the small objects have finite volume, voxels, that each contain numerous molecules of moving fluids and rock.

NRMI experiments

The NMRI experiments were performed at the laboratory of New Mexico Resonance, Albuquerque, New Mexico, using a 1.89 Tesla horizontal-bore, superconducting magnet equipped with shielded gradient coils. In a 1.89 Tesla static field, the Lamor frequency of the proton in the nucleus of a molecule of freshwater is approximately 80.35 MHz. A custom-built, high-pass birdcage (Watkins and Fukushima, 1988) was used as a radio-frequency probe. Spin-echo, spin-warp imaging (Callaghan, 1991) was performed with an echo time of 4 milliseconds (ms) and repetition times of 50-100 ms. Since these repetition times are shorter than the spin-lattice relaxation time of water, low-angle pulses were used for excitation, and spoiling gradients were applied during the recycle time. Vertical image slices were collected with imaging gradients all less then 2 Gauss/cm.

Velocity experiments

Using the epoxy model based upon sample ML-1, we developed a system to measure the three Cartesian components of the velocity of water flowing slowly through the modeled Ophiomorpha macroporosity. Using a peristaltic pump and a constant head reservoir, we created a recirculating flow system through the model. The two values of specific discharge simulated in the experiments, 0.00025 m/s and 0.00013 m/s, are less than the tracer velocity of approximately 0.0045 m/s observed during a forced-gradient tracer test by Renken et al. (2005a) that used rhodamine WT and deuterium. Whereas values for both specific discharge and tracer velocity are less than the interstitial velocity, both are apparent velocities that characterize the bulk advection of water.

The low velocities in these experiments required a phase-encoded, stimulated-echo, velocity method (Fukushima, 1999). Using a stimulated echo allows us to track the motion for a relatively long time, compared to more typical spin-echo methods. Each velocity component is encoded in the phase difference between a pair of images. The image matrix is 128 pixels along the z-axis and 32 pixels in both the x- and y-axes. Four signal averages of each image took 76 minutes to acquire. Data processing for these velocity experiments continues, and no results are presented in this paper.

Tracer experiments

Preceding the NRMI experiments on the matrix porosity, two limestone samples, ML-2 and ML-3, were dried in a vacuum oven and then submerged in D_2O for 2 days with intermittent partial vacuum applied. The matrix porosity of sample ML-2 absorbed 2.0 mL of D_2O, weighing 14.5 g dry and 16.7 g saturated (Table 1). Likewise, the matrix porosity of sample ML-3 absorbed 155 mL of D_2O, weighing 729.0 g dry and 900.5 g saturated (Table 1). Following weighing, each sample was placed in an acrylic chamber. In the case of ML-2, shaped vaguely like a pyramid (Figure 3A), the chamber was filled with freshwater spiked with trace amounts of Gd-DTPA and left in static conditions (Table 1). A second sample chamber held sample ML-3, a roughly cylindrical solid (Figure 3B). This chamber was connected to a constant-head reservoir and functioned as a flow-through cell with a specific discharge of 0.00025 m/s maintained by a peristaltic pump (Table 1).

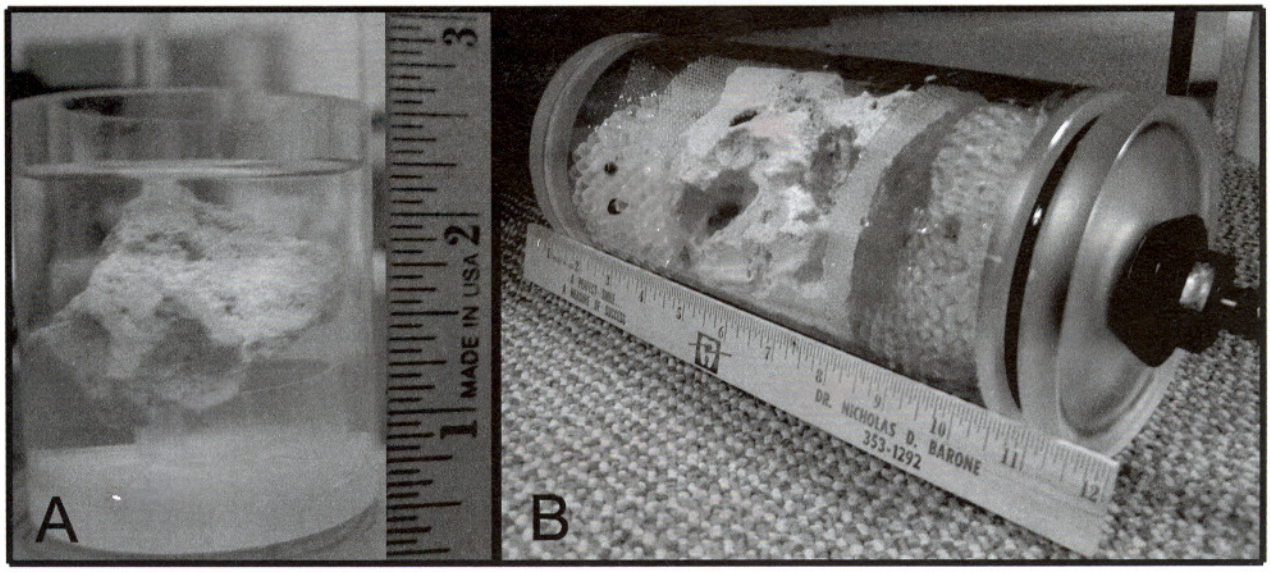

Figure 3. Samples ML-2 (A) and ML-3 (B) within experimental acrylic chambers. Ruler is scaled in inches. Freshwater surrounds both samples, which are saturated with D2O. The chamber containing ML-2 remained in static conditions during the experiment. The chamber containing ML-3 served as a flow cell set to a constant discharge of 2 mL/sec. The glass beads on either side of sample ML-3 act to smooth and straighten flow lines entering and leaving the chamber.

Two NMRI experiments were run for 48 and 21 hours using samples ML-2 and ML-3, respectively (Table 1). The 2-dimensional images collected in these two experiments represent a slice parallel to the long axis of the samples and through the centroid of the samples. The slice thickness measured approximately 3 mm for ML-2 and 6 mm for ML-3 (Table 1). Slice thickness for ML-2 was thinner because of an increase of signal strength related to the presence of Gd-DTPA. For both experiments, the field of view measures 6 x 6 cm with 128 pixels in the plane of the z-axis and 256 pixels in the plane of the y-axis. Each image of the average NMRI signal strength represents the composite of four images, each eight minutes in duration, collected during a 24-minute period. The NMRI signal strength in each voxel of the tracer experiments corresponds to the relative proportions of freshwater, D_2O, and rock matrix.

RESULTS FROM THE TRACER EXPERIMENTS

Sequential time-step NMRI images recorded in the two tracer experiments show the progressive displacement of D_2O by either Gd-DTPA-spiked freshwater, in the case of ML-2, or freshwater for ML-3 (Figures 4 and 5). Very little difference in "mapped" signal strength is visible between images during the first few hours of both experiments; however, differences are substantial between the beginning and end of both experiments (Figures 4 and 5). For example, after 48 hours, the signal strength of the Gd-DTPA-spiked freshwater in the matrix porosity of ML-2 was 13% of the Gd-DTPA-spiked freshwater surrounding the sample (Figure 6). In the experiment with sample ML-3, signal strength increased 150% after 21 hours of freshwater flowing past the sample (Figure 7). The rate of change in signal strength in sample ML-2 decreases over the course of the experiment (Figure 6). The rate of change in signal strength in sample ML-3 was greatest during the first 30 minutes of the experiment and is nearly constant during the remaining time (Figure 7).

The rate at which freshwater and D_2O move between the matrix and surrounding voids is spatially non-uniform. In both samples ML-2 and ML-3, serial images reveal areas of the samples that saturate with freshwater quickly and other regions that never change in signal strength, indicating very little or no influx of freshwater (Figures 4 and 5).

Volumetric removal of D_2O

Sample ML-2 contains 5.3 cm3 of rock and a matrix porosity of 38% (Table 1). It seems that Gd-DTPA-spiked freshwater replaced 34% of the 2 mL of D_2O contained within the matrix porosity within 48 hours, a rate of 0.001 milliliters per hour per gram of sample (mL/hr-g) (Table 1). Since this experiment was conducted in static, non-flowing conditions, the primary controls on the displacement of D_2O within sample ML-2 was by (1) the density difference between the Gd-DTPA-spiked freshwater and D_2O, and (2) molecular diffusion. By the end of the experiment on ML-2, a slight contrast in NMRI signal strength developed in the chamber between the top and bottom of the

Table 1. Sample properties, experimental settings, and results.

	Value	Method of calculation	ML - 2	ML - 3
A	Sample shape (approximate)		Pyramid	Cylinder
B	Density (g/cm^3)	Measured	2.73	2.73
C	Dry weight (g)	Measured	14.5	729.0
D	Saturated weight (g)	Measured	16.7	900.5
E	Initial vol of D_2O (mL)	(D-C)/1.107	2.0	155.0
F	Volume of rock (cm^3)	C/B	5.3	267.0
G	Porosity (%)	E/F	38	58
H	Sample deminsons (cm) (approximate)	Measured	Base = 3 Height = 2.5	Length = 8 Diameter = 10
I	Surface area (cm^2) (approximate)	Based on H	26.4	> 250
J	Sample volume (cm^3)	E+F	7.3	422.0
K	Surface area to volume ratio	I/J	3.6	1 > 0.6
L	Specific discharge (m/s)	Measured	0	0.00025
M	Concentration of Gd-DTPA solution (%)	Measured	0.25	0.0
N	Experiment duration (hrs)	Measured	48	21
O	image slice thickness (mm)	Measured	3	6
P	Sample weight at end of experiment (g)	Measured	16.67	889.5
Q	Fraction of D_2O removed (%)	(D-P)/(D-(C+E))	34	67
R	Vol of D_2O removed (mL)	QXE	0.7	103.0
S	Rate of D_2O removal (mL/hr-g)	(R/N)/C	0.001	0.07

surrounding fluid (Figure 4). This layering of signal strength points to greater concentrations of D_2O in the bottom of the chamber as it leaked from the bottom of the sample.

Similarly, sample ML-3 contains 267 cm^3 of rock and a matrix porosity of 58% (Table 1). Macropores separated from the touching vugs, yet saturated with D_2O, likely contribute to the larger measurement of matrix porosity. Fluid-weight differences at the beginning and end of the experiment on sample ML-3 indicate that freshwater replaced approximately 67% of the 155 mL of D_2O after 21 hours, a rate of 0.07 mL/hr-g (Table 1). Despite the much shorter time span of the experiment with sample ML-3, the effect of flowing water is clearly evident; the volume of D_2O replaced in sample ML-3 (103 mL) is two orders of magnitude greater than that in sample ML-2 (0.7 mL), which has a much lower surface area to volume ratio (Table 1). We speculate that if given the 48 hours allotted to the static, non-flowing experiment, virtually all D_2O in sample ML-3 would be replaced with freshwater.

DISCUSSION AND RELEVANCE OF THE TRACER EXPERIMENTS

The images produced using NMRI during the experiments on samples of rock from the Biscayne aquifer shed light on the transport properties of one type of rock matrix within this eogenetic karst aquifer. Our tracer experiments demonstrate that the exchange of fluids into and out of a matrix composed of a peloid-ooid grainstone occurs readily, even when driven principally by density gradients and diffusion. Freshwater flowing past the outer wall of the matrix and through the macropores that penetrate the samples greatly magnifies the infiltration into the matrix, even using relatively low groundwater velocities.

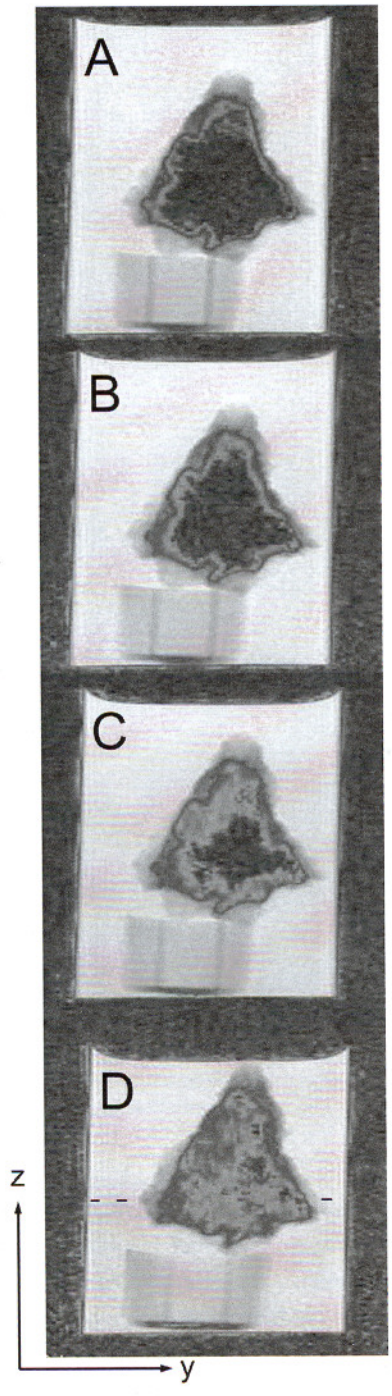

Figure 4. Progressive NMRI images from a 3-mm-thick slice through the center of ML-2 during the static experiment (note the y- and z-axis orientations – width of images is 6 cm). t = time. A) t = 0, B) t = 1.5 hrs, C) t = 18 hrs, D) t = 48 hrs. Brighter areas of the image correlate to greater concentrations of freshwater. The average freshwater saturation of the sample after 48 hrs measures approximately 13%. Note that some parts of the sample lose D_2O more rapidly than other areas. Also note that after 48 hrs, a slight contrast in NMRI signal strength has developed between the top and bottom of the surrounding fluid, an indication of denser D_2O collecting in the lower part of the chamber (indicated by a dashed line).

Also clearly demonstrated in these experiments are spatial variations in the rate of fluid exchange between the matrix and surrounding void that are probably controlled by permeability heterogeneities in the matrix. The peloid-ooid-dominated lithofacies of samples ML-2 and ML-3 has a tropical, shallow-marine, subtidal depositional origin and hase undergone significant post-depositional bioturbation and subsequent meteoric diagenesis (Tedesco and Wanless, 1991; Curran, 2007). Therefore, the regions that do not change NRMI signal strength in Figures 4 and 5 may represent areas of the sample where interparticle space is occluded by micrite or carbonate cements and thus is not susceptible to freshwater infiltration within the detection limits of the two experiments.

Since D_2O and saltwater are slightly denser than freshwater – 10% and 3%, respectively – and are also miscible with freshwater, these particular experiments may serve as a comparable study for removing denser, saline waters from the rock matrix of coastal, eogenetic karst aquifers that are affected by saltwater intrusion. The Biscayne continues to experience problems with saltwater intrusion, though of lesser extent than during the 1950s and early 1960s (Renken et al., 2005b; Langevin, 2001; Sonenshein and Koszalka, 1996; Klein and Ratzlaff, 1989). Despite the difference in density between D_2O and saltwater, D_2O produces no NMRI signal and therefore is preferred over saltwater, which produces a strong NMRI signal, to reveal the migration of freshwater into the samples.

Our experiment on ML-3 in the flow cell simulates the displacement of a conservative tracer from a part of the aquifer matrix. These results certainly do not apply to parts of the aquifer that dominated solely by porous media flow or other matrix types of lower permeability. In effect, the lateral migration of saltwater within a carbonate aquifer composed of vertically stacked, carbonate, high-frequency cycles and associated stratiform zones of high permeability, such as documented for part of the Biscayne aquifer (Cunningham et al., 2006a,b), is similar to the "bottle brush" permeability distribution described by Vacher et al. (2006) for the Upper Floridan aquifer with respect to aquifer storage and recovery. Thus, the freshwater-saltwater mixing zone is likely more complex than can be resolved by observational data and simulated in regional-scale density-dependent models (e.g., Kohout, 1960; Langevin, 2001). If present in the coastal area, the stratiform flow zones of touching-vug porosity similar to that contained in sample ML-1 or shown in Figure 1 could be preferentially affected during initial landward intrusion of saltwater, and those zones may possibly be the first part of the aquifer system to experience recovery.

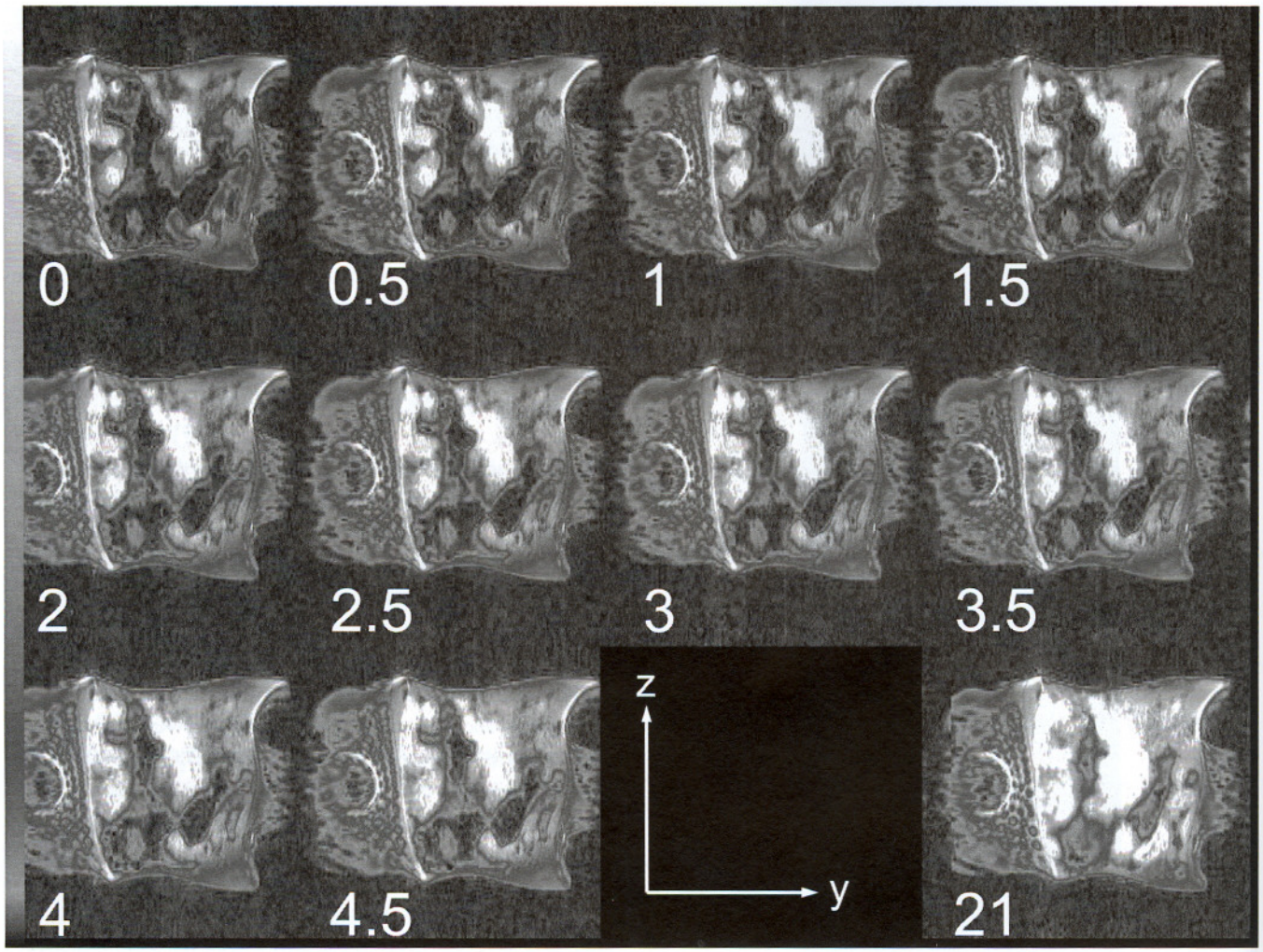

Figure 5. Progressive NMRI images from a 6-mm-thick slice through the center of ML-3 during the flow-cell experiment (note the y- and z-axis orientations – width of images is 6 cm). Numbers refer to hours from the beginning of the experiment. Brighter areas of the image correlate with greater concentrations of freshwater. The glass beads used to straighten and smooth the flow lines are visible on either side of the sample. Image warping increases from the center of the image, where the field lines from the static magnetic field are most parallel. Note the lengthy gap in data between 4.5 hrs and 21 hrs when no images were collected overnight. Changes in the NMRI signal strength are almost imperceptible between consecutive images; however, the cumulative loss of D_2O is clearly visible after 4.5 hrs. After 21 hrs, 67% of the D_2O has been replaced by freshwater.

Our NMRI experiments are relevant to two modern programs of artificial recharge in the limestone aquifers of south Florida: saltwater-intrusion barriers and aquifer storage and recovery. In each of these programs, the flux of fluid through the matrix porosity must be within some range for project feasibility. NMRI methods provide an excellent, non-invasive tool to make empirical measurements of fluid flux on field samples and could serve as a scoping tool for cost-benefit analyses.

1) Saltwater-intrusion barriers – Artificial recharge of the Biscayne aquifer has been proposed as a means of installation of salinity-barrier systems to retard landward encroachment of saltwater (e.g., Missimer International, Inc., 1998; Missimer et al., 2000). One of the unknowns in salinity-barrier design is the rate at which saltwater is replaced by freshwater in the small-scale matrix porosity of limestone.

2) Aquifer storage and recovery (ASR) – Several ASR projects in south Florida rely on the applicability of injecting freshwater (often reclaimed water from treatment facilities) into the confined portions of the Floridan aquifer for later withdrawal and use, particularly in connection with the multibillion-dollar Comprehensive Everglades Restoration Project (Reese, 2002). Vacher et al. (2006) caution that heterogeneities in the small-scale matrix porosity of limestone greatly affect location of stored freshwater, both after injection and recovery.

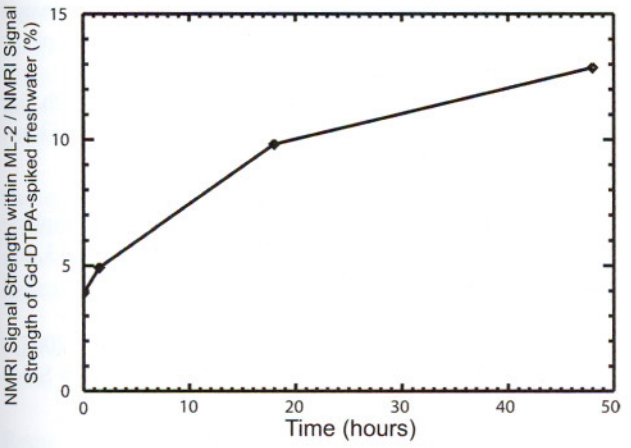

Figure 6. Fractional NMRI signal strength within sample ML-2 compared to the NMRI signal strength in the Gd-DTPA-spiked freshwater surrounding the sample. The rate of D_2O loss from the sample decreases during the course of the experiment.

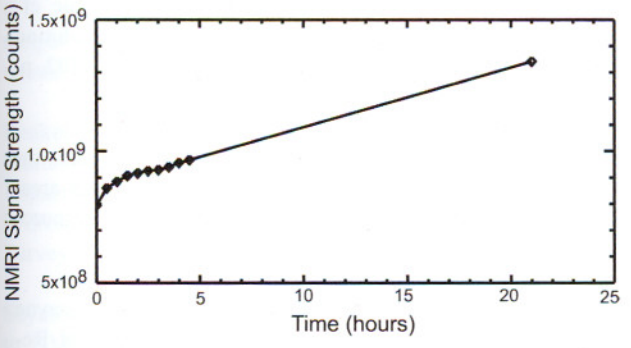

Figure 7. NMRI signal strength as a function of time from the flow-cell experiment on ML-3. Note the lengthy gap in data when no images were collected overnight. The rate of D_2O loss from the sample is greatest during the first 30 minutes of the experiment and is nearly constant during the rest of the experiment.

Finally, given our results, it seems that restoring freshwater in the very permeable portions of the Biscayne aquifer intruded by saltwater may proceed rapidly. Assuming that hydraulic gradients of freshwater between the Everglades and Biscayne Bay can be maintained is a water-management challenge for southeast Florida. The area suffers from the effects of roughly a century of urbanization, increased water-use demands, threats of sea-level rise, and periodic droughts.

CONCLUSIONS

In this study, we investigated properties of groundwater flow through three samples of peloid-ooid grainstone from a preferred flow zone of biogenic touching-vug porosity within the late Pleistocene limestones that comprise the Biscayne aquifer. In particular, we presented innovative methods of X-ray computed tomography, rapid prototyping, and nuclear magnetic resonance imaging to visualize flow within the touching vugs in a non-invasive manner. We also investigated the migration of freshwater into Biscayne rock matrix saturated with D_2O. Sequential time-step NMRI images revealed the exchange of D_2O and either freshwater or Gd-DTPA-spiked freshwater between rock matrix and surrounding macroporosity. The images highlight the rate at which the denser D_2O is replaced with freshwater in this porous and permeable limestone. Specifically, we measured rates upward of 0.001 mL/hr per gram of sample in static conditions where density-dependant flow and diffusion drive the fluid exchange, and perhaps as great as 0.07 mL/hr per gram of sample when freshwater continuously flows past the sample at velocities less than those found within stressed areas of the Biscayne aquifer. Since D_2O and saltwater are both slightly denser than freshwater, these results may shed light on the process of displacement of saltwater in aquifers that have experienced saltwater intrusion. More specifically, these results may simulate the restoration of matrix porosity within preferred groundwater-flow zones of a coastal, eogenetic karst aquifer in which solutes are removed from a rock matrix saturated with saltwater.

ACKNOWLEDGMENTS

Principal funding for this project came through a USGS Mendenhall Postdoctoral Fellowship to Florea. Collection of geologic data for the Biscayne aquifer was funded in part by grants to Cunningham by the Priority Ecosystems Science program of the USGS and Critical Ecosystems Studies Initiative program of Everglades National Park. Greg Murphy at Mark Two Engineering, Inc. in Miami provided specific counsel and expertise during the design and construction of the epoxy model. Eiichi Fukushima of ABQMR provided specific insight and guidance during the design of the NMRI experiments. Joann Dixon of the USGS assisted with the visualization and alteration of the STL files as well as the design of the physical model. John Mylroie of Mississippi State University and Melissa Hill of the Southwest Florida Water Management District provided insightful reviews of an earlier draft of this manuscript. Any use of trade names is for descriptive purposes only and does not imply endorsement by the U.S Government.

REFERENCES

Budd, D.A., and Vacher, H.L., 2004, Matrix permeability of the confined Floridan Aquifer: Hydrogeology Journal, v. 12, no. 5, p. 531–549.

Callaghan, P.T., 1991, Principles of Nuclear Magnetic Resonance Microscopy: Clarendon Press, Oxford, 516 p.

Chang, C.T.P., and Watson, A.T., 1999, NMR imaging of flow velocity in porous media: AIChE Journal v. 45, no. 3, p. 437-444.

Cressler, A., 1993, The caves of Dade County, Florida: Georgia Underground, Dogwood City Grotto, Inc., of the National Speleological Society, Inc., v. 30, no. 3, p. 9-16.

Cunningham, K.J., 2004, Application of ground-penetrating radar, digital optical borehole images, and core for characterization of porosity and paleokarst in the Biscayne aquifer, southeastern Florida, USA: Journal of Applied Geophysics, v. 55, p. 77-90.

Cunningham, K.J., Carlson, J.L., Wingard, G.L., Robinson, E., and Wacker, M.A., 2004a, Characterization of Aquifer Heterogeneity Using Cyclostratigraphy and Geophysical Methods in the Upper Part of the Karstic Biscayne Aquifer, Southeastern Florida: U.S. Geological Survey Water Resources Investigation Report 03-4208, 66 p.

Cunningham, K.J., Wacker, M.A., Robinson, E., Gefvert, C.J., and Krupa, S.L., 2004b, Hydrogeology and ground-water flow at Levee-31N, Miami-Dade County, Florida, Jul. 2003-May 2004: U.S. Geological Survey Scientific Investigations Map I-2846, 1 pl.

Cunningham, K.J., Renken, R.A., Wacker, M.A., Zygnerski, M.R., Robinson, E., Shapiro, A.M., and Wingard, G.L., 2006a, Application of carbonate cyclostratigraphy and borehole geophysics to delineate porosity and preferential flow in the karst limestone of the Biscayne aquifer, SE Florida: In Harmon, R.S., and Wicks, C., eds., Perspectives on Karst Geomorphology, Hydrology, and Geochemistry— A Tribute Volume to Derek C. Ford and William B. White: Geological Society of America Special Paper 404, p. 191-208, doi:10.1130/2006.2404(16).

Cunningham, K.J., Wacker, M.A., Robinson, E., Dixon, J.F., and Wingard, G.L., 2006b, A cyclostratigraphic and borehole geophysical approach to development of a three-dimensional conceptual hydrogeologic model of the karstic Biscayne aquifer, southeastern Florida: U.S. Geological Survey Scientific Investigations Report 2005-5235, 69 p.

Cunningham, K.J., and Curran, H.A., 2007, Ichnogenic porosity, high-frequency cyclostratigraphy, and groundwater flow in the karst Biscayne aquifer, SE Florida, USA: In Zonneveld, J.-J., and Gingras, M.K., eds., International Ichnofabrics Workshop IX Abstracts with Program, Calgary, Alberta, Canada, p. 12-15.

Curran, H.A., 2007, Ichnofacies, ichnocoenoses, and ichnofabrics of Quaternary shallow-marine to dunal tropical carbonates: a model and implications: In Miller, W., III, ed., Trace Fossils: Concepts, Problems, Prospects: Elsevier, p. 232-247.

Fish, J.E., and Stewart, M., 1991, Hydrogeology of the surficial aquifer system, Dade County, Florida: U.S. Geological Survey Water-Resources Investigations Report 90-4108, 50 p., 11 pls.

Florea, L.J., 2006, The Karst of West-Central Florida: Ph.D. dissertation, Department of Geology, University of South Florida, Tampa, 523 p.

Florea, L.J., and Vacher, H.L., 2006, Springflow hydrographs: Eogenetic vs. telogenetic karst: Ground Water, v. 44, no. 3, p. 352–361.

Florea, L.J., Vacher, H.L., Donahue, B., and Naar, D., 2007, Quaternary cave levels in peninsular Florida: Quaternary Science Reviews, v. 26, p. 1344-1361.

Fukushima, E., 1999, Nuclear magnetic resonance as a tool to study flow: Annual Review of Fluid Mechanics, v. 31, p. 95-123.

Ketcham, R.A., and Iturrino, G.J., 2005, Nondestructive high-resolution visualization and measurement of anisotropic effective porosity in complex lithologies using high-resolution X-ray computed tomography: Journal of Hydrology v. 302, p. 92-106.

Klein, H., and Ratzlaff, K.W., 1989, Changes in saltwater intrusion in the Biscayne aquifer, Hialeah-Miami Springs area, Dade County, Florida. U.S: Geological Survey Water-Resources Investigations Report 87-4249, 1 sheet.

Kohout, F.A., 1960, Cyclic flow of salt water in the Biscayne aquifer of southeastern Florida: Journal of Geophysical Research, v. 65, no. 7, p. 2133-2141.

Langevin, C.D., 2001, Simulation of ground-water discharge to Biscayne Bay, southeastern Florida: U.S. Geological Survey Water-Resources Investigations Report 00-4251, 127 p., 3 pls.

Lucia, F.J., 1995, Rock fabric/petrophysical classification of carbonate pore space for reservoir characterization: American Association of Petroleum Geologists Bulletin, v. 79, p. 1275-1300.

Martin, J.B., and Dean, R.W., 2001, Exchange of water between conduits and matrix in the Floridan aquifer: Chemical Geology, v. 179, p. 145–165, doi: 10.1016/S0009-2541(01)00320-5.

Missimer, T.M., Maliva, R.G., Walker, C.W., and Owosina, E., 2000, Anatomy of a nearshore mixed siliciclastic-carbonate deposit, the Plio-Pleistocene of southern Broward County, Florida: Gulf Coast Association of Geological Societies Transactions, v. L, p. 111-128.

Missimer International, Inc., 1998, Hollywood coastal salinity barrier pilot project. Second phase drilling-Interium Technical Memorandum: Consultants report to the City of Hollywood, Florida, 130 p.

Mylroie, J.E., Carew, J.L., and Vacher, H.L., 1995, Karst development in the Bahamas and Bermuda: In Curran, H.A. and White, B., eds., Terrestrial and Shallow Marine Geology of the Bahamas and Bermuda: Geological Society of America Special Paper, Boulder, Colorado, v. 300, p. 251-267.

Parker, G.G., Ferguson, G.E., Love, S.K., and others, 1955, Water resources of southeastern Florida, with special reference to the geology and ground water of the Miami area: U.S. Geological Survey Water-Supply Paper 1255, 965 p.

Pullman, P., 2007, His Dark Materials: Alfred A. Knopf, New York. 933 pp.

Reese, R.S., 2002, Inventory and review of aquifer storage and recovery in southern Florida: U.S. Geological Survey Water-Resources Investigations Report 02-4036.

Renken, R.A., Cunningham, K.J., Zygnerski, M.R., Wacker, M.A., Shapiro, A.M., Harvey, R.W., Metge, D.W., Osborn, C.L., and Ryan, J.N., 2005a, Assessing vulnerability of a municipal well field to contamination in a karst aquifer: Environmental & Engineering Geoscience, v. 4, p. 319-331.

Renken, R.A., Dixon, J., Koehmstedt, J., Ishman, S., Lietz, A.C., Marella, R.L., Telis, P., Rogers, J., and Memberg, S., 2005b, Impact of anthropogenic development on coastal ground-water hydrology in southeastern Florida, 1900-2000: U.S. Geological Survey Circular 1275, 77 p.

Seymour, J.D, and Callaghan, P.T., 1997, Generalized approach to NMR analysis of flow and dispersion in porous media: AIChE Journal, v. 43, no. 8, p. 2096-2111.

Shattuck, M.D., Behringer, R.P., Johnson, G.A., and Georgiadis, J.G., 1997, Convection and flow in porous media. Part 1. Visualization by magnetic resonance imaging: Journal of Fluid Mechanics, v. 332, p. 215-245.

Smart, P.L., Beddows, P.A., Coke, J., Doerr, S., Smith, S., and Whitaker, F.F., 2006, Cave development on the Caribbean coast of the Yucatan Peninsula, Quintana Roo, Mexico: In Harmon, R.S., and Wicks, C., eds., Perspectives on Karst Geomorphology, Hydrology, and Geochemistry—A Tribute Volume to Derek C. Ford and William B. White: Geological Society of America Special Paper 404, p. 105-128, doi:10.1130/2006.2404(10).

Sonenshein, R.S., and Koszalka, E.J., 1996, Trends in water-table altitude (1984-93) and saltwater intrusion (1974-93) in the Biscayne aquifer, Dade County, Florida: U.S. Geological Survey Open-File Report 95-705, 2 sheets.

Tedesco, L.P., and Wanless, H.R., 1991, Generation of sedimentary fabrics and facies by repetitive excavation and storm infilling of burrow networks: Holocene of south Florida and Caicos Platform, B.W.I.: PALAIOS, v. 6, p. 326-343.

Tessier, J.J., Packer, K.J., Thovert, J.-F., and Adler, P.M., 1997, NMR measurements and numerical simulation of fluid transport in porous solids: AIChE Journal, v. 43, no. 7, p. 1653-1661.

Vacher, H.L., and Mylroie, J.L., 2002, Eogenetic karst from the perspective of an equivalent porous medium: Carbonates and Evaporites, v. 17, no. 2, p. 182–196.

Vacher, H.L., Hutchings, W.C., and Budd, D.A., 2006, Metaphors and models: The ASR bubble in the Floridan aquifer: Ground Water, v. 44, no. 2, p. 144-154.

Watkins, J.C., and Fukushima, E., 1988, The highpass birdcage coil for NMR: Review of Scientific Instrumentation, v. 59, p. 926-929.

Worthington, S.R.H., Ford, D.C., and Beddows, P.A., 2000, Porosity and permeability enhancement in unconfined carbonate aquifers as a result of solution: In Speleogenesis: Evolution of Karst Aquifers, Klimchouk, A., Ford, D., Palmer, A., and Dreybrodt, W., eds. 463–472, National Speleological Society, Huntsville.